Modelling and Control of Tidal Energy Conversion Systems with Long Distance Converters

Modelling and Control of Tidal Energy Conversion Systems with Long Distance Converters

M C Sousounis, J K H Shek*, M A Mueller**

**Institute for Energy Systems, School of Engineering, The University of Edinburgh, United Kingdom*
M.Sousounis@ed.ac.uk

Keywords: Tidal energy system, direct torque control, long distance drives, induction generator.

Abstract

In order to optimise a tidal energy conversion system operation, maintenance and power generation aspects have to be taken into account. As a result the key focus of this paper is to propose and investigate an alternative method of implementing a tidal energy conversion system using a pitch-regulated turbine and a variable-speed squirrel cage induction generator with long distance converters. The generator power output can be optimised by utilising variable-speed control strategies allowing the system to operate at maximum power coefficient while availability can be increased by reducing the components installed offshore by using long three-phase cables between the generator and onshore voltage source converters. The tidal current energy conversion system is investigated by developing a full resource-to-grid model in MATLAB/Simulink and by performing system analysis regarding the effects of harmonics. Simulation results show that by manipulating the harmonic components, by adding passive filters, the problems associated with the harmonics and the reflecting voltage waves in the cables can be minimised.

1 Introduction

The potential to generate carbon free power from the world's tides is evident. The UK alone has a significant tidal current energy resource which can supply 29% of the UK electricity demand based on 2012 statistics [1, 2]. Moreover, a study has estimated that the energy available in tidal currents could supply 14.25TWh per year using 'first-generation' technology options without significantly impacting the underlying resource [3]. From the massive tidal energy resource in the UK waters only 18TWh per year of the total energy has been assessed as being economically recoverable with today's technologies [4]. At certain locations tidal currents can possess very high energy density which can lead to large amounts of power. As a result of high energy density, devices are subjected to large forces in order to maximise conversion of the available energy. Still, tidal current devices are expected to operate reliably under harsh conditions and even though they have similarities to offshore wind turbines in many aspects, a number of characteristics differentiate the approach needed regarding power transmission and drive-train design. Some of these characteristics are: predictable direction and speed of the tidal current, predetermined available area in a tidal channel, less swept area due higher density of water, continuous underwater operation and smaller distances to shore [5].

To be more specific, the continuous underwater operation requires that the tidal system must work reliably with high availability. This dictates that onsite visits must be reduced to a minimum since tidal devices are usually installed at locations with high tidal currents. At these locations, the windows of opportunity for onsite visits are relatively short (often less than one hour), which means that major operations need to be extremely quick or be able to continue in high tidal flows [5]. Another aspect of tidal arrays that affect power transmission is that they will be close enough to shore and therefore offshore substations and high-voltage subsea transmission can be avoided. Eliminating the equipment which is installed offshore can consequently reduce the offshore maintenance. In this context, it has been suggested that tidal energy developers can extend the availability of their systems by moving the power electronics from the nacelle to the shore. This could reduce onsite visits since the failure frequency of power converters can be significant based on data from onshore wind turbines [6]. Locating the power electronics on land means that the generator has to be controlled using long subsea cables and therefore long distance drives are needed. Long distance converters have been used to drive electrical submersible pumps (ESPs) in oil offshore platforms.

The literature regarding long distance drives focuses on the variable speed operation of low power motors [7 - 11] which are usually designed to be used as pumps in offshore oil platforms [9 - 13]. The main points discussed are the reasons behind the appearance of over-voltages at the terminals of motors with long feeders [7, 9], filtering techniques in order to mitigate the problems associated with the long feeders [7, 8], the importance of accurate frequency domain analysis in order to investigate system resonant frequency in different topologies [10] and [8] also discusses the effect of long cables in a PWM vector controller.

Currently, tidal current turbine developers have not yet decided on the optimal tidal current conversion system

(TCCS) and therefore a number of different designs appear [12]. Most of the designs are bottom mounted, with low solidity blades and horizontal axis rotors, while the approaches differ in generator technology. Dominant choices are direct drive generators or geared permanent magnet synchronous generators (PMSGs) and squirrel cage induction generators (SCIGs). Power limitation is achieved using fixed pitch or variable pitch blades. Research papers are focused on the power limitation mechanisms [13, 14], grid integration of tidal current conversion systems [15] and power capture maximisation control methods [16].

The aim of this paper is to present a full resource-to-grid dynamic model of a single tidal current turbine with the proposed long distance converters. The system is based on a three-bladed tidal turbine with pitch-regulated blades and a SCIG controlled using direct torque control with space vector modulation (DTC SVM). Utilising the model, the applicability of long distance converters in tidal current systems will be investigated and ways to mitigate the challenges associated with them such as high harmonics and over-voltages will be presented. In section 2 the modelling of the tidal resource, tidal turbine power characteristics, pitch controller, generator controller and the grid side are briefly explained. Section 3 shows the results from the simulation of the reference model and finally in section 4 frequency domain system analysis is performed regarding the effects of passive harmonic filters in the tidal current conversion system with long distance converters.

2 Modelling of tidal current conversion system

In this section all the modelling aspects of a tidal current conversion system will be described. The proposed topology can be seen in Figure 1.

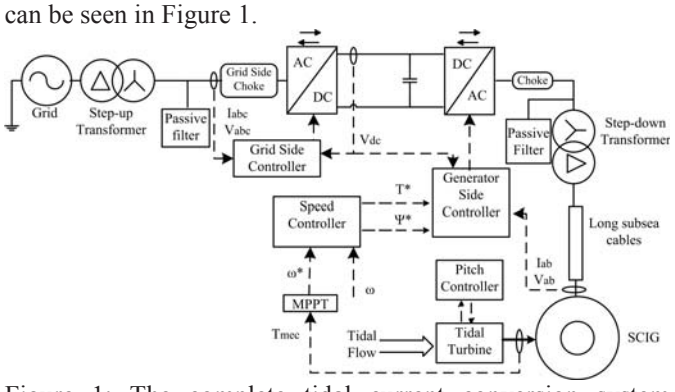

Figure 1: The complete tidal current conversion system modelled

The tidal turbine shaft is connected to the SCIG rotor through a gearbox. The output of the medium voltage generator is transmitted to shore by long three-phase subsea cables. The medium voltage is transformed to low voltage using an onshore transformer. Before the voltage source converter (VSC) filters are installed. The importance of the filtering method will be discussed later. The DTC SVM method enables variable speed operation of the SCIG. On the grid side, the low voltage output of the inverter is first filtered and then a step-up transformer is used in order to match the grid high voltage.

2.1 Tidal resource

The power potential of tidal currents can be derived by the same formula as for wind energy systems.

$$P_{tide} = 0.5 \cdot \rho_{water} \cdot A \cdot V_{current}^{3} \quad (1)$$

Where ρ_{water} is the sea water density approximately equal to 1025kg·m^{-3}, A is the swept area by the tidal turbine blades and $V_{current}$ is the fluid speed in m/s.

As input to the model a half-cycle with high peak flow speed was chosen in order to represent the most complex period of operation of the system. The tidal current speed used is shown in Figure 2.

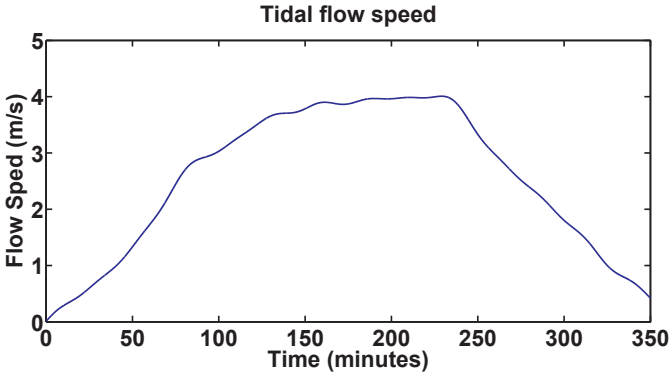

Figure 2: Tidal current speed used as input to the system

2.2 Tidal turbine model

The model is based on the steady-state power characteristics of the turbine. The output power of the turbine is given by the following equation.

$$P_m = C_p(\lambda,\beta) \cdot P_{tide} \quad (2)$$

Where P_m is the mechanical output power of the turbine in watts and $C_p(\lambda,\beta)$ is the power coefficient of the turbine which is a function of the tip speed ratio, λ, and blade pitch angle, β. In this model a maximum C_p of 0.48 is assumed. The turbine power characteristics can be seen in Figure 3 [17].

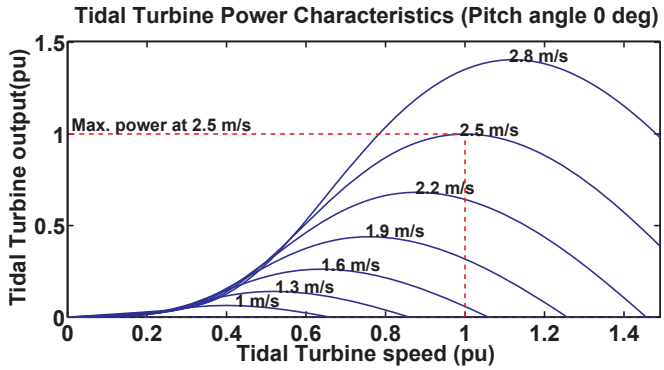

Figure 3: Tidal turbine power output versus turbine speed at different tidal current speeds

2.3 Pitch controller

Power limitation in high tidal current speeds is achieved by using pitch angle control. This action corresponds to changing the pitch value such that the leading edge of the blade is moved into the flow increasing the angle of attack and thus inducing a blade feathering effect. The control structure of the pitching system developed can be observed in Figure 4. The pitching mechanism limits the turbine speed to rated speed by reducing C_p in equation (2) and so reducing the mechanical power captured.

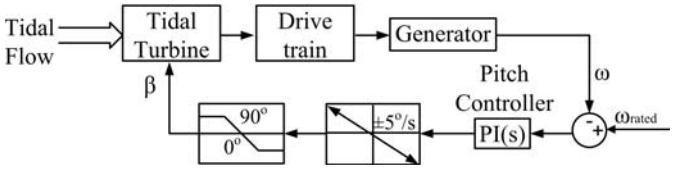

Figure 4: Pitch controller structure based on turbine speed

2.4 Generator Controller

In order to ensure variable speed operation the SCIG is controlled from an onshore VSC using DTC SVM. The DTC SVM methods are based on the classical DTC [18] but they also operate at constant switching frequency. From the family of DTC SVM methods the DTC SVM scheme with closed-loop torque and flux control in stator flux coordinates has been implemented [19]. The control structure of the DTC SVM method modelled can be seen in Figure 5.

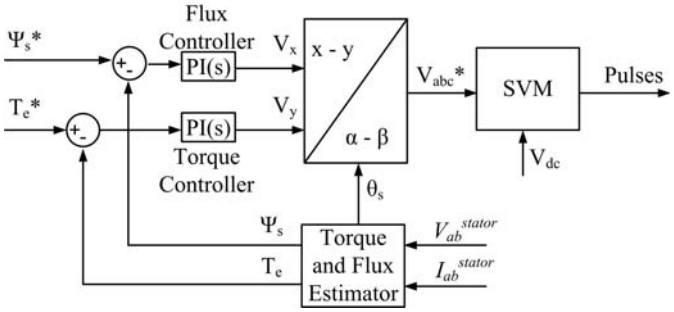

Figure 5: DTC SVM method with closed-loop torque and flux control in stator flux coordinates

The block diagram of the flux and torque estimator and the SVM can be seen in Figure 6 and Figure 7 respectively.

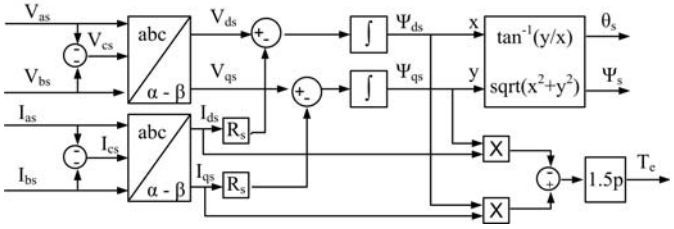

Figure 6: Block diagram of the flux and torque estimator

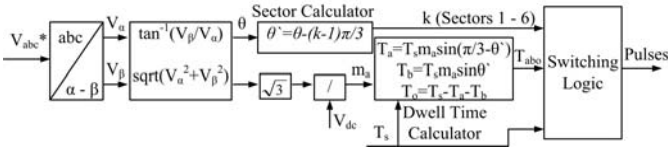

Figure 7: Block diagram of the Space Vector Modulation method modelled [20]

2.5 Grid side modelling

The power generated by the TCCS is delivered to the grid through a VSC. The grid-tied inverter is connected to the grid through a line reactor, which helps to reduce line current distortion, a filter that reduces harmonics and a step-up transformer from 690V to 11kV. The inverter is controlled by a PWM scheme called voltage oriented control (VOC) with decoupled controllers [20] which ensures a constant DC link voltage of $1100V_{dc}$, constant frequency output of 50Hz on the AC side and control over the amount of reactive power flowing based on grid requirements. The equations that describe the output of the VOC with decoupled controllers are:

$$v_{di} = -PI(s)\cdot(i^{*}_{dg} - i_{dg}) + \omega_g \cdot L_g \cdot i_{qg} + v_{dg} \quad (5)$$

$$v_{qi} = -PI(s)\cdot(i^{*}_{qg} - i_{qg}) - \omega_g \cdot L_g \cdot i_{dg} + v_{qg} \quad (6)$$

Based on equations (5) and (6) the control structure implemented can be seen in Figure 8.

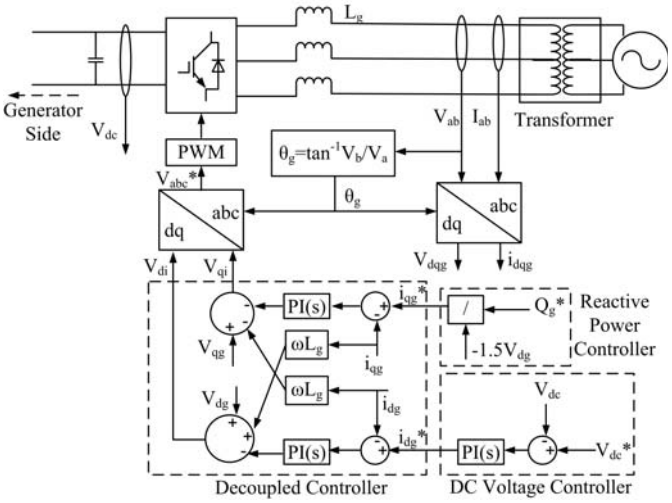

Figure 8: Control structure of the grid side controller

3 Reference model simulation results

In this section the operation of the proposed TCCS will be demonstrated. In order to do so a reference model was developed with the following characteristics:

- Cable model: PI section
- Cable length: 3.5km
- Passive filter with single tuning at 250Hz and quality factor of 2
- Reactive power of 80kVAr

In Figure 9 the power generated by the SCIG, the pitch angle and the generator speed in a 350 minutes simulation can be observed. Until a certain generator speed is reached no power is produced because system losses will be significant compared to the power generated. After a certain speed is reached, approximately 0.25pu at 38 minutes, the generator is connected to the grid. Between 38 and 77 minutes the generator speed follows the maximum power point curve of the turbine in order to achieve maximum C_p until maximum generator speed is reached. At maximum speed, approximately 1.002pu, and since tidal flow continues to increase, the pitch angle starts to increase. There is a small period of time between 77 and 80 minutes where maximum speed is reached but torque still increases to match rated power. At 80 minutes rated power is reached. From that point and onwards as tidal current speed increases, the pitch angle also increases to limit mechanical torque input and keep power constant. Accordingly, when tidal flow decreases pitch angle decreases to zero and the generator is disconnected when generator speed is below 0.25pu.

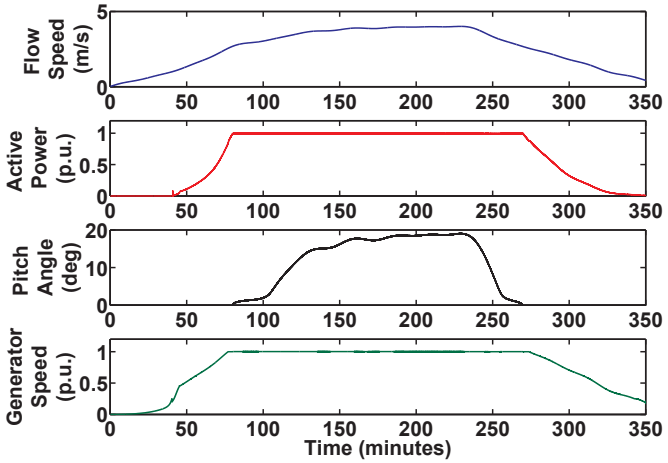

Figure 9: Flow speed, power generated, pitch angle and generator speed during a half tidal cycle.

4 Frequency-domain system analyses

In order to explore the ways the long cables affect the TCCS different cases regarding cable modelling and filter design are considered. These cases are described in Table 1 where PI cable model and distributed parameter line (DPL) cable model are compared when different filters are used. Based on these cases, the system impedance versus frequency will be investigated in order to identify the changes in resonant frequencies and how the harmonics components can cause over-voltages at the generator terminals.

Case	*Cable Model*	*Filter type*
1	PI	None
2	PI	Single tuned
3	PI	C-type
4	DPL	Single tuned

Table 1: Cases considered for the frequency-domain analysis.

In all cases the tuned frequency is 250Hz, the quality factor is 2, reactive power is 80kVAr and the cable length is 3.5km. Also, the frequency domain analysis is performed when rated power is generated.

By performing frequency-domain analysis in case 1 the harmonic components that distort the voltage at the generator terminals can be identified. The results of the fast Fourier transform (FFT) can be seen in Figure 10.

Observing Figure 10 predictable results are produced by the FFT. Major harmonic components appear at even multiples of the fundamental operating frequency of the generator, which is approximately 50Hz at rated power. Also, significant harmonic components appear near the multiples of the operating frequency of the VSC, which is 2500Hz, plus and minus the multiples of the fundamental frequency.

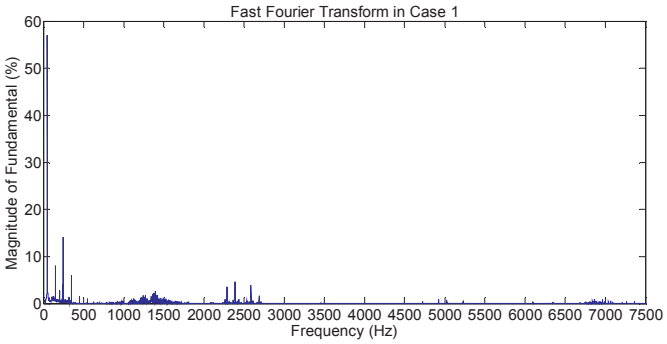

Figure 10: Fast Fourier transform of the voltage at generator terminals in case 1.

By adding passive harmonic filters at the inverter output the harmonic components at the generator terminals can be filtered. Table 2 shows the changes in voltage total harmonic distortion at the generator terminals (VTHDm) and at the low voltage side of the generator transformer (VTHDmt) for each case studied.

Case	*VTHDm (%)*	*VTHDmt (%)*
1	41.37	54.11
2	10.25	38.5
3	8.21	27.46
4	10.31	39.38

Table 2: Voltage total harmonic distortion at the generator terminals and at the low voltage side of the generator transformer for each case studied.

Apart from the mitigation of low order harmonics, the addition of passive filters can change the impedance paths of high order harmonics which, if not properly damped, can cause overvoltage at machine terminals because of the reflecting voltage waves in the cables as discussed in the literature referenced in section 1.

Therefore in order to understand the appearance of over-voltages, which can be seen in Figure 11 for each case, the impedance for a given frequency is calculated at generator terminals, as seen in Figure 12, shows the impedance paths

for each frequency. If a frequency component has a low impedance path to the filter then this harmonic component is filtered. Respectively, if a frequency component has a high impedance path to the filter then the harmonic component is not filtered as expected. This can help in identifying system resonant frequencies which must be avoided. Also it gives a comprehensive view of how impedance can change at each frequency from the addition of passive filters or by changing the cable model.

In Figure 11 it can be observed that without the addition of a passive filter (case 1), an overvoltage higher than 1.2pu appears which can cause insulation damage and lead to a fault. With the addition of a passive filter harmonics are reduced to desirable levels for the generator side.

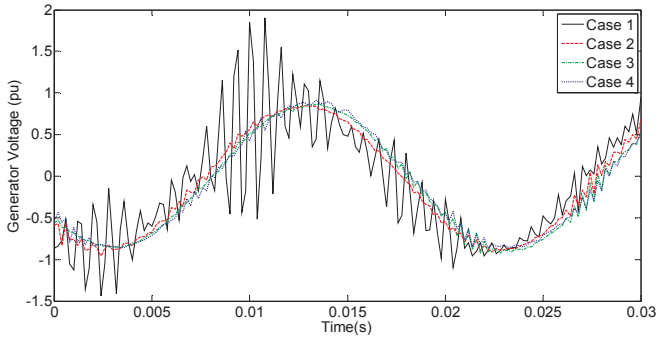

Figure 11: Voltage at the generator terminals during rated operation for each case.

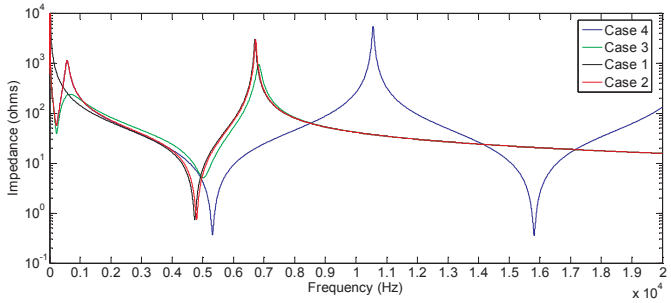

Figure 12: Filter impedance versus frequency graph for each case.

In Figure 12 the filter impedance versus frequency as calculated from the generator terminals can be observed. All the components of the system affect this graph, however filter and cable choice affect the number of zeroes and poles.

At frequencies higher than 4000Hz zeroes and poles appear because of the long cables. In the case of a single PI section (cases 1,2 and 3) a zero appears at approximately 4800Hz. Depending on the filter chosen the position and the magnitude of the zero can change but not significantly. The single PI section model also has a pole at approximately 6700Hz with the exact position and magnitude to be affected by filter design as well. In case 3, the C-type filter reduces the effect of the zero and pole. On the other hand, when DPL cable model was used multiple zeroes and poles appear at specific steps which can be calculated as shown in equation (6):

$$F_{DPL} = 1/\left(4 \cdot d \cdot \sqrt{L_c \cdot C_c}\right) \quad (6)$$

Where d is the cable length, L_c is the cable inductance per unit length and C_c is the cable capacitance per unit length. With L_c = 0.594mH/km and C_c = 0.31μF/km zeroes and poles appear every approximately 5266Hz. In both cases, PI section model and DPL, a low impedance path appears near 5000Hz which is two times the operating frequency of the active rectifier and harmonics should appear but as shown in Figure 10 these harmonics have very low magnitude.

At frequencies lower than 4000Hz, shown in Figure 13, the filter tuned at 250Hz has a great effect in creating a low impedance path at the specific frequency. The C-type filter (case 3) creates an even lower impedance path and this is why the VTHD is lower. In cases 2 and 4, where the same filters are used but different cable models, the results are identical showing that the cable model has no effect at low frequencies. At the fundamental frequency, cases 2, 3 and 4 create a lower impedance path compared to case 1 and this is the reason why the filter introduces extra losses to the system.

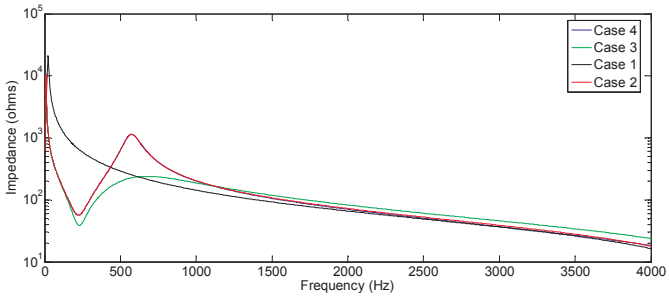

Figure 13: Filter impedance versus frequency graph for each case at frequencies below 4000Hz.

Apart from the zero created by the filters at the tuned frequency, single tuned filters (cases 2 and 4) create a small pole as well. On the other hand, the C-type filter impedance smoothens after the zero. For frequencies between 1000Hz and 4000Hz, the C-type filter has higher impedance compared to all other cases making it less efficient at this range.

5 Conclusion

An alternative way of integrating TCCS was proposed using long distance controls. System components were explained in detail. A reference model was developed in order to demonstrate the ability of the proposed system to operate using measured tidal current speed. Analysis focused on the frequency domain of the system since high harmonic components flowing in the cables can cause overvoltage to the generator terminals. For that purpose a single tuned and a C-type filter were used. In addition, the PI section cable model and the distributed parameter line cable model were compared in the proposed system. Impedance versus frequency graphs were used in order to demonstrate the effects of different filters and cable models used. Based on the simulated results the proposed system cannot operate

without adding a filter at the rectifier output because of the overvoltage at generator terminals. Future research will focus on the challenges introduced when longer cables are used and harsh site conditions such as high turbulence and wake effects affect system operation.

Acknowledgements

The authors would like to thank ANDRITZ Hydro Hammerfest and The University of Edinburgh for funding this project.

References

[1] Department of Energy and Climate Change. 2013, July. UK ENERGY IN BRIEF 2013. A National Statistics Publication. Available: https://www.gov.uk/

[2] The Crown Estate. 2012, October. UK Wave and Tidal Key Resource Areas Project Summary Report: Version 2. Available: www.thecrownestate.co.uk

[3] A. Sankaran Iyer, S. J. Couch, G. P. Harrison, and A. R. Wallace. "Phasing of tidal current energy around the UK and potential contribution to electricity generation." *European Wave and Tidal Energy Conference*, Southampton, UK, 2011.

[4] Black & Veatch. 2005, June. Phase II UK Tidal Stream Energy Resource Assessment. Issue 1. Available: http://www.carbontrust.com

[5] D. Krohn, M. Woods, J. Adams, B. Valpy, F. Jones and P. Gardner. "Wave and Tidal Energy in the UK: Conquering Challenges, Generating Growth," renewableUK. Document Version: Issue 2, February 2013.

[6] F. Spinato, P. J. Tavner, G. J. W. van Bussel, and E. Koutoulakos, "Reliability of wind turbine subassemblies," *IET Renew. Power Gener.*, vol. 3, no. 4, p. 387, 2009.

[7] A. von Jouanne, D. A. Rendusara, P. N. Enjeti, and J. W. Gray, "Filtering techniques to minimize the effect of long motor leads on PWM inverter-fed AC motor drive systems," *IEEE Trans. Ind. Appl.*, vol. 32, no. 4, pp. 919–926, 1996.

[8] A. K. Abdelsalam, M. I. Masoud, S. J. Finney, and B. W. Williams, "Vector control PWM-VSI induction motor drive with a long motor feeder: performance analysis of line filter networks," *IET Electr. Power Appl.*, vol. 5, no. 5, p. 443, 2011.

[9] R. M. Tallam, G. L. Skibinski, T. A. Shudarek, and R. A. Lukaszewski, "Integrated Differential-Mode and Common-Mode Filter to Mitigate the Effects of Long Motor Leads on AC Drives," *IEEE Trans. Ind. Appl.*, vol. 47, no. 5, pp. 2075–2083, Sep. 2011.

[10] S. O. Faried and O. Ilochonwu, "Subsea Cable Applications in Electrical Submersible Pump Systems," *IEEE Trans. Ind. Appl.*, vol. 46, no. 2, pp. 575–583, 2010.

[11] A. C. S. De Lima, H. W. Dommel, and R. M. Stephan, "Modeling adjustable-speed drives with long feeders," *IEEE Trans. Ind. Electron.*, vol. 47, no. 3, pp. 549–556, Jun. 2000.

[12] SI-OCEAN. 2012, December. Ocean Energy: State of the Art. Available: http://www.si-ocean.eu

[13] B. Whitby and C. Ugalde-Loo, "Performance of Pitch and Stall Regulated Tidal Stream Turbines," *IEEE Trans. Sustain. Energy*, vol. PP, no. 99, pp. 1–9, 2013.

[14] Z. Zhou, F. Scuiller, J. F. Charpentier, M. Benbouzid, and T. Tang, "Power limitation control for a PMSG-based marine current turbine at high tidal speed and strong sea state," in *2013 International Electric Machines & Drives Conference*, 2013, pp. 75–80.

[15] M. Kuschke, S. Pertzsch, and K. Strunz, "Modeling of tidal energy conversion systems for primary response testing," in *2012 IEEE Power and Energy Society General Meeting*, 2012, pp. 1–6.

[16] S. E. Ben Elghali, M. E. H. Benbouzid, J. F. Charpentier, T. Ahmed-Ali, and I. Munteanu, "High-order sliding mode control of a Marine Current Turbine driven Permanent Magnet Synchronous Generator," in *2009 IEEE International Electric Machines and Drives Conference*, 2009, pp. 1541–1546.

[17] S. Heier, "Wind Energy Conversion Systems," in *Grid Integration of Wind Energy Conversion Systems*, 1st ed. Chichester, UK: John Wiley & Sons, Inc. 1998, ch. 2. sec. 2.1.5, pp. 38 – 43.

[18] I. Takahashi and T. Noguchi, "A New Quick-Response and High-Efficiency Control Strategy of an Induction Motor," *IEEE Trans. Ind. Appl.*, vol. IA-22, no. 5, pp. 820–827, Sep. 1986.

[19] Y. Xue, X. Xu, T. G. Habetler, and D. M. Divan, "A low cost stator flux oriented voltage source variable speed drive," in *Conference Record of the 1990 IEEE Industry Applications Society Annual Meeting*, pp. 410–415.

[20] B. Wu, Y. Lang, N. Zargari, and S. Kouro, "Power Converters in Wind Energy Conversion Systems," in *Power Conversion and Control of Wind Energy Systems*,. Hoboken, New Jersey: John Wiley & Sons, Inc. 2011, ch. 4. pp. 87 – 152.